PARITY-VIOLATING ELECTRON SCATTERING

KRISHNA S. KUMAR

Department of Physics, University of Massachusetts, Amherst, MA 01003, USA

ABSTRACT

We describe the technique of fixed target parity-violating electron scattering, in which weak neutral current amplitudes between electrons and target nuclei are measured in order to probe novel properties of nuclear matter. We focus on two modern applications: as a sensitive probe of the strange quark content of the nucleon and as a precise measurement of the neutron RMS radius of a heavy nucleus.

1 Introduction

In order to understand the physics of parity-violating electron scattering, it is useful to begin by reviewing the symmetries of the electroweak interaction, which in turn have been firmly established over the last few decades via precision measurements of electromagnetic, weak charged current and weak neutral current interactions among elementary particles.

Symmetries have played a major role in our understanding of fundamental interactions in Nature since the dawn of subatomic physics in the 1890s. As our understanding of subatomic structure developed rapidly with the birth of quantum mechanics and the incorporation of special relativity, it was realized that exact symmetries of nature are deeply interconnected with fundamental conservation laws. In physics, a symmetry implies that the Lagrangian or Hamiltonian describing the system under study is invariant under the transformation of a generalized coordinate. An exact symmetry of the Lagrangian is related to the conservation of an observable. For example, translational symmetry implies linear momentum conservation and rotational symmetry implies angular momentum conservation.

The concept of internal symmetries of the Lagrangian of elementary particles has given us a fundamental understanding of the origin of strong, weak and electromagnetic interactions. In these lectures, we show how we exploit our precise knowledge of the electroweak interactions of leptons and quarks to probe nucleons and nuclei in novel ways. The basic technique is the use polarized electron scattering off fixed targets to measure parity-violating asymmetries, thus accessing the neutral weak interaction amplitude between electrons and target particles.

We begin with a brief introduction to the symmetries of the electroweak Lagrangian that allows us to derive the electroweak charges of leptons and quarks. We then describe the formalism of probing nuclear and nucleon structure using fixed-target electron scattering, with particular emphasis on parity-violation. This is followed by an introduction to the experimental technique of parity-violating electron scattering to measure weak neutral current amplitudes. We then focus on the two main applications, which are the search for strangeness in nucleons and the measurement of the neutron rms radius in a heavy nucleus. We finally conclude with a summary of the current status of the subfield and an outlook to the future.

2 The Symmetries of the Electroweak Interaction

The electroweak interaction arises from the imposition of local gauge invariance to the free particle Lagrangian, which contains left-handed fermions in weak isospin doublets and right-handed fermions in iso-singlets. The specific gauge group that is chosen is $SU(2)_L \times U(1)_Y$, which results in the emergence of 4 electroweak gauge bosons, two charged and two neutral, that mediate the electroweak interaction. The charged bosons ($W^\pm$) mediate the charged weak interactions which have the well-known $V - A$ structure. We then require that one of the neutral gauge bosons must be the massless photon with the known electromagnetic couplings to various fermions. In addition, we now impose spontaneous breakdown of the gauge symmetry via the HIggs mechanism and we are led to the second neutral boson (Z^0), with specific predictions for the weak neutral couplings to various fermions as well as a prediction for the Z^0 boson mass with respect to that of the W boson in terms of a single new parameter: the electroweak mixing angle θ_W.

The resulting neutral electroweak charges of the light quarks and leptons are given in Table 1. Both left- and right- handed particles have weak neutral current charges, which can in turn be expressed as vector and axial-vector charges. The weak neutral current interaction has been extensively studied in high energy collider experiments and the electroweak charges listed in Table 1

Table 1: Electromagnetic and neutral weak charges of the electron and light quarks. The helicity charges are given by $g^R = g^V + g^A$ and $g^L = g^V - g^A$.

Particle	q^{em}	g^V	g^A
e^-	-1	$-\frac{1}{4} + \sin^2 \theta_W$	$\frac{1}{4}$
u	$\frac{2}{3}$	$\frac{1}{4} - \frac{2}{3}\sin^2 \theta_W$	$-\frac{1}{4}$
d, s	$-\frac{1}{3}$	$-\frac{1}{4} + \frac{1}{3}\sin^2 \theta_W$	$\frac{1}{4}$

have been extensively tested. The value of the weak mixing angle is known to very high precision: the world average value, extrapolated to the energy scale of the mass of the Z boson, is 0.23116 ± 0.00013 [1]. As we shall see in following sections, the weak neutral current interaction provides complementary information to the electromagnetic interaction due to the fact that the ratio of weak charges is different from the corresponding ratio of electromagnetic charges.

3 Parity-Violating Electron Scattering

3.1 Introduction

Since the weak neutral charge of electrons and light quarks are different for left- and right-handed particles, the parity symmetry is violated in the scattering of polarized electrons off unpolarized targets. In this section, we introduce the formalism for a quantitative discussion of parity violating electron scattering, following the discussion in an early review of the topic **??**. We begin with the case of potential scattering, where the theory is most transparent. Potential scattering is a reasonable approximation for the practical case of scattering from a spinless, isoscalar target such as ^{12}C or ^{4}He.

We will then discuss elastic scattering from the proton. The results are more complicated because the non-zero proton spin gives rise to several form factors as opposed to the single form factor required to describe isoscalar, spinless nuclei. Finally, we will discuss elastic scattering off a heavy nucleus to measure the neutron rms distribution.

3.2 Potential Scattering

We start with potential scattering in the Born approximation. The target is a spinless potential distribution fixed in space while the electron is treated ultra-relativistically. To fix our notation, we first discuss purely electromagnetic scattering. Consider an electron of energy E scattered by an angle θ with momentum transfer $q = 2E \sin(\theta/2)$. The potential corresponds to a spatial charge distribution $\rho(r)$ which is the Fourier transform of the electromagnetic form factor

$$F(q) = \int d^3 r \rho(r) \exp[i\mathbf{q} \cdot \mathbf{r}]. \tag{1}$$

The cross section is given by

$$\frac{d\sigma}{d\Omega} = |f(\theta)|^2 \cos^2(\theta/2) \tag{2}$$

where the scattering amplitude $f(\theta)$ may be written

$$f(\theta) = \frac{2\alpha}{q^2} F(q).$$ (3)

The scattering amplitude has two factors. The first is the form factor $F(q)$ which describes the spatial distribution of the charge. The second is $2\alpha/q^2$ which is the amplitude for scattering from a point distribution characterized by the following potential:

$$V(r) = \frac{e^2}{4\pi r}.$$ (4)

In order to include weak scattering, the potential must be generalized as follows:

$$V(r) = ke^2 g^B g^T \frac{\exp[-Mr]}{4\pi r}$$ (5)

where g^B is the charge of the incident beam particle and g^T is the charge of the target particle in units of the electron charge e. Also k is the strength of the coupling and M is the mass of the exchanged particle: $M = 0$ for the electromagnetic interaction and $M = M_Z$ for the neutral weak current. The constant $k = 1$ for electromagnetism and $k = (\sin\theta_W \cos\theta_W)^2$ for weak scattering.

One central feature of *longitudinally polarized* electron scattering is that the weak charge of a relativistic electron depends on its helicity. Thus $g^R \neq g^L$, where $g^R(g^L)$ is the charge of an electron with right(left) helicity. In discussing neutral weak amplitudes, it is more convenient to discuss vector and axial-vector weak charges, which are just linear combinations of the left- and right-handed weak charges: $g^R = g^V + g^A$ and $g^L = g^V - g^A$. The weak and electromagnetic charges of the electrons and relevant quarks are given in Table 1.

The other key feature of Table 1 is that the relative sizes of the weak and electromagnetic charges of the the quarks are different. Since we are averaging over target particle spin, the vector charge g^V is the relevant weak charge. The up quark has the strongest electromagnetic charge whereas the down and strange quarks have the strongest weak vector charge. The net result is that the charge distribution in an extended potential as seen by an electromagnetic probe might be quite different from the charge distribution seen by a weak probe of the same extended potential.

A convenient way to describe the various charge distributions is to use a *number* density $\rho_i(r)$ for each quark flavor i and a corresponding form factor

$$F_i(q) = \int d^3r \rho_i(r) \exp[i\mathbf{q}\cdot\mathbf{r}].$$ (6)

Then all electromagnetic and weak scattering from a given potential may be described by the same three F_i. The scattering amplitude $f(q)$ is given by the general form:

$$f(q) = -\frac{1}{2\pi}\int V(\mathbf{r})\exp[i\mathbf{q}\cdot\mathbf{r}]d^3r = \frac{(2k\alpha g^B g^T)}{(q^2 + M^2)}F(q).$$ (7)

As in the electromagnetic case, each scattering amplitude factors into two pieces, a form factor describing the spatial distribution of the quarks and a piece describing the point-like interaction. The cross section is given by the coherent sum of all scattering amplitudes $f_i(q)$

$$\frac{d\sigma}{d\Omega} = \sum |f_i(\theta)|^2 \cos^2(\theta/2)$$ (8)

The sum of amplitudes includes all quarks contributing to the potential and both weak and electromagnetic interactions.

For ordinary electromagnetic scattering, $q \ll M_Z$, the weak interaction is negligible, and only one combination of the quark form factors survives:

$$F_\gamma = \sum g_i^{em} F_i = \frac{2}{3} F_u - \frac{1}{3}(F_d + F_s) \tag{9}$$

To experimentally isolate the contribution from each of the three flavors, measurements of weak scattering amplitudes are required, which we discuss next.

3.3 Parity Violation

The most practical way to measure the weak amplitude in electron scattering is to measure the asymmetry

$$A^{PV} = \frac{d\sigma_R - d\sigma_L}{d\sigma_R + d\sigma_L} \tag{10}$$

If A^{PV} is non-zero, it constitutes parity violation and is dominated by the interference between the weak and electromagnetic amplitudes.

The cross section is proportional to the square of the scattering amplitudes:

$$f^R = f_\gamma + f_Z^R, \qquad f^L = f_\gamma + f_Z^L \tag{11}$$

where

$$f_\gamma(\theta) = -\frac{2\alpha}{q^2} \sum q_j^{em} F_j(q); \;\; f_Z^{L(R)}(\theta) = \frac{2\alpha k_Z g^{L(R)}}{M_Z^2} \sum g_j^V F_j(q) \tag{12}$$

Here, $g^{L(R)}$ is the weak charge of the electron, g_i^V is the vector charge of the ith quark flavor, and $k_Z = (\sin\theta_W \cos\theta_W)^{-2}$. The asymmetry is

$$A^{PV} = \frac{|f^R|^2 - |f^L|^2}{|f^R|^2 + |f^L|^2} \simeq \frac{f_\gamma(f_Z^R - f_Z^L)}{f_\gamma^2} = \frac{f_Z^R - f_Z^L}{f_\gamma} \tag{13}$$

This equation gives the essence of the parity-violating asymmetry. The weak-electromagnetic interference gives rise to a ratio of *amplitudes* rather than the ratio of the squares of the amplitudes. Since $g^R - g^L = 2g^A = 1/2$, we have

$$f_Z^R - f_Z^L = \frac{\alpha k_Z}{M_Z^2} \sum g_j^V F_j(q). \tag{14}$$

When the weak and electromagnetic charges for the quarks are included, we get:

$$
\begin{aligned}
A^{PV} &= -\frac{k_Z q^2}{2M_Z^2} \frac{\sum g_j^V F_j}{\sum q_j F_j} \\
&= -\frac{k_Z q^2}{2M_Z^2} \frac{(\frac{1}{4} - \frac{2}{3}\sin^2\theta_W)F_u + (-\frac{1}{4} + \frac{1}{3}\sin^2\theta_W)(F_d + F_s)}{\frac{2}{3}F_u - \frac{1}{3}(F_d + F_s)}
\end{aligned}
\tag{15}
$$

A measurement of A^{PV} thus provides one more combination of form factors such as that in Eqn. 9.

To isolate F_s, one more equation is needed. For a spinless $I = 0$ nucleus such as ^{4}He or ^{12}C, the distribution of up and down quarks must be identical. For these cases, we have the equation

$$F_u = F_d \equiv F \tag{16}$$

By combining this with Eqn. 15, we obtain:

$$
\begin{aligned}
A^{PV} &= -\frac{k_Z q^2}{2M_Z^2} \left(\frac{-\frac{1}{3}\sin^2\theta_W (F - F_s) - \frac{1}{4}F_s}{\frac{1}{3}(F - F_s)} \right) \\
&= \frac{k_Z q^2}{2M_Z^2} \left(\sin^2\theta_W + \frac{F_s}{4F_\gamma} \right)
\end{aligned}
\tag{17}
$$

where F_γ is defined in Eqn. 9. This is a very important formula. On the one hand, if the Q of the reaction is small enough such that F_s can be neglected, the asymmetry is independent of hadronic structure and A^{PV} can be used to precisely test the assumptions of the standard model. On the other hand at larger values of q, the asymmetry provides a clean measure of F_s.

3.4   Nucleon Scattering

Extending the above method to relativistic nucleons is straightforward. Instead of the three-momentum transfer q, we use the four-momentum transfer squared Q^2. The most general possible current for elastic electron nucleon scattering assuming current conservation, Lorentz invariance, and time reversal is

$$j_\mu^a(proton) = \langle p(k', s')|j_\mu^a|p(k,s)\rangle =$$

$$\overline{u}(k', s')\left[F_1^a(Q^2)\gamma_\mu + \frac{i}{2M}F_2^a(Q^2)\sigma_{\mu\nu}q^\nu + F_A^a(Q^2)\gamma_\mu\gamma^5 + F_P^a(Q^2)\gamma^5 q_\mu \right]u(k,s) \tag{18}$$

where the $F^{a'}s$ are real Dirac form factors that depend only upon Q^2. There are four currents since the target particle can be a proton or a neutron and the current can be electromagnetic or weak. The index a shall be used to denote both characteristics.

Formulas for cross sections and asymmetries are usually expressed in terms of the Sachs form factors defined by:

$$G_E^a \equiv F_1^a - \tau F_2^a; \quad G_M^a \equiv F_1^a + F_2^a \tag{19}$$

where $\tau = Q^2/4M$. The differential cross section for electron scattering from the proton is then

$$\left.\frac{d\sigma}{d\Omega}\right|_{lab} = \left(\frac{\alpha^2}{4E^2\sin^4\frac{\theta}{2}} \right)\frac{E'}{E}\left\{ \frac{(G_E^{p\gamma})^2 + \tau(G_M^{p\gamma})^2}{1+\tau}\cos^2\frac{\theta}{2} + 2\tau(G_M^{p\gamma})^2\sin^2\frac{\theta}{2} \right\}. \tag{20}$$

The neutron cross section is given by changing the superscript p to n.

The parity-violating asymmetry is given by

$$A^{PV} = \frac{\sigma_R - \sigma_L}{\sigma_R + \sigma_L} = \left[\frac{-G_F Q^2}{\pi\alpha\sqrt{2}} \right] \tag{21}$$

$$\times \frac{\varepsilon G_E^{p\gamma} G_E^{pZ} + \tau G_M^{p\gamma} G_M^{pZ} - \frac{1}{2}(1 - 4\sin^2\theta_W)\varepsilon' G_M^{p\gamma} G_A^{pZ}}{\varepsilon(G_E^{p\gamma})^2 + \tau(G_M^{p\gamma})^2}$$

where $\varepsilon = [1 + 2(1+\tau)\tan^2(\theta/2)]^{-1}$ is the transverse polarization of the virtual photon exchanged and $\varepsilon' = \sqrt{\tau(1+\tau)(1-\varepsilon^2)}$. An important feature of this result is that the asymmetry at backward

angles involves the axial form factor G_A^{pZ} even though the target is unpolarized. The reason is that helicity is conserved, so that the relevant coupling at backward angles is $g_b^R g_t^R (g_b^L g_t^L)$ for right(left) handed electrons. Then the difference between the couplings of right- and left-handed electron $g_b^R g_t^R - g_b^L g_t^L = -2(g_b^V g_t^A + g_b^A g_t^V)$. This introduces an axial term and, as discussed below, the radiative corrections of this term are quite significant.

The above results involve many form factors. However, as for the case of potential scattering discussed above, we can relate all of the form factors to a few *flavor form factors* as follows:

$$\langle p | j_\mu^a | p \rangle = \langle p | \sum g_i^{Va} \overline{u}_i \gamma_\mu u_i | p \rangle + \langle p | \sum g_i^{Aa} \overline{u}_i \gamma_\mu \gamma_5 u_i | p \rangle$$

$$= \overline{u}_p \sum \left[g_i^{Va} \left(F_1^i \gamma_\mu + \frac{i}{2M} F_2^i \sigma_{\mu\nu} q^\nu \right) + g_i^{Aa} F_A^i \gamma_\mu \gamma_5 \right] u_p \tag{22}$$

where g_i^a is the coupling of the current by boson a to quark i. The spinor of the proton is denoted u_p and the spinors of the quarks are denoted u_i. Thus the flavor form factors are defined:

$$\langle p | \overline{u}_i \gamma_\mu u_i | p \rangle = \overline{u}_p \left(F_1^i \gamma_\mu + \frac{i}{2M} F_2^i \sigma_{\mu\nu} q^\nu \right) u_p$$

$$\langle p | \overline{u}_i \gamma_\mu \gamma^5 u_i | p \rangle = \overline{u}_p F_A^i \gamma_\mu \gamma^5 u_p \tag{23}$$

There are a total of nine flavor form factors since there are three flavors times three Lorentz invariants:

$$F_1^u, \quad F_2^u, \quad F_A^u$$
$$F_1^d, \quad F_2^d, \quad F_A^d$$
$$F_1^s, \quad F_2^s, \quad F_A^s \tag{24}$$

To include neutron scattering with the same set of form factors, we invoke charge symmetry:

$$p \to n \quad \Rightarrow \quad u \to d,\ d \to u,\ s \to s. \tag{25}$$

This implies the analog of Eqn. 16:

$$F_1^u \equiv F_1^{pu} = F_1^{nd}; \quad F_1^d \equiv F_1^{pd} = F_1^{nu}; \quad F_1^s \equiv F_1^{ps} = F_1^{ns} \tag{26}$$

This is the analog of setting $F_u = F_d$ for the $I = 0$ case given above.

The weak and electromagnetic currents may be expressed in terms of these flavor form factors for the proton as follows. The electromagnetic current in term of quarks is

$$j_\mu^\gamma = \frac{2}{3} \overline{u} \gamma_\mu u - \frac{1}{3} \overline{d} \gamma_\mu d + \frac{2}{3} \overline{c} \gamma_\mu c - \frac{1}{3} \overline{s} \gamma_\mu s + \cdots.$$

Thus by Eqns. 22 and 22

$$F_i^{p\gamma} = \frac{2}{3} F_i^u - \frac{1}{3} F_i^d - \frac{1}{3} F_i^s; \quad F_i^{n\gamma} = \frac{2}{3} F_i^d - \frac{1}{3} F_i^u - \frac{1}{3} F_i^s. \tag{27}$$

Similarly for the weak current

$$\begin{aligned} j_\mu^Z &= (\frac{1}{4} - \frac{2}{3} \sin^2 \theta_W) \overline{u} \gamma_\mu u - (\frac{1}{4} - \frac{1}{3} \sin^2 \theta_W) \overline{d} \gamma_\mu d \\ &+ (\frac{1}{4} - \frac{2}{3} \sin^2 \theta_W) \overline{c} \gamma_\mu c - (\frac{1}{4} - \frac{1}{3} \sin^2 \theta_W) \overline{s} \gamma_\mu s \\ &- \frac{1}{4} \overline{u} \gamma_\mu \gamma_5 u + \frac{1}{4} \overline{d} \gamma_\mu \gamma_5 d - \frac{1}{4} \overline{c} \gamma_\mu \gamma_5 c + \frac{1}{4} \overline{s} \gamma_\mu \gamma_5 s \end{aligned} \tag{28}$$

Consequently:

$$F_i^{pZ} = (\frac{1}{4} - \frac{2}{3}\sin^2\theta_W)F_i^u - (\frac{1}{4} - \frac{1}{3}\sin^2\theta_W)(F_i^d + F_i^s) \tag{29}$$

With Eqns. 27 and 29 elastic electron, neutrino, and antineutrino scattering and parity-violating electron scattering from either the proton and neutron can be described by the same set of form factors.

Any non-singular linear combination of the F_i^u, F_i^d, and F_i^s may be used for expressing cross sections and asymmetries. The best known form factors are G_E^γ and G_M^γ for the proton and neutron. Thus it is traditional to use $G_{E,M}^{p\gamma}$, $G_{E,M}^{n\gamma}$, and $G_{E,M}^s$ as the independent form factors. In terms of these quantities,

$$G_{E,M}^{pZ} = \frac{1}{4}(G_{E,M}^{p\gamma} - G_{E,M}^{n\gamma}) - \sin^2\theta_W G_{E,M}^{p\gamma} - \frac{1}{4}G_{E,M}^s \tag{30}$$

There is a firm prediction for A^{PV} if strangeness is neglected. Any deviation of the measured asymmetry from the prediction could then be attributable to non-zero strange form factors. The equation for extracting strange form factors from A^{PV} and electromagnetic scattering data, is given by

$$A^{PV} = \left[\frac{-G_F M_p^2 \tau}{\pi\alpha\sqrt{2}}\right]\left\{(1 - 4\sin^2\theta_W) - \right. \tag{31}$$

$$\frac{[\varepsilon G_E^{p\gamma}(G_E^{n\gamma} + G_E^s) + \tau G_M^{p\gamma}(G_M^{n\gamma} + G_M^s)]}{\varepsilon(G_E^{p\gamma})^2 + \tau(G_M^{p\gamma})^2} -$$

$$\left. \frac{(1 - 4\sin^2\theta_W)\sqrt{\tau(1+\tau)}\sqrt{1-\varepsilon^2}G_M^{p\gamma}(-G_A^{(1)} + \frac{1}{2}F_A^s)}{\varepsilon(G_E^{p\gamma})^2 + \tau(G_M^{p\gamma})^2}\right\}$$

3.5 Scattering off ^{208}Pb

In this section we illustrate how parity violating electron scattering measures the neutron density, mirroring the discussion in Ref. [2]. For simplicity, this section uses the plane-wave Born approximation and neglects nucleon form factors. These are necessary for a quantitative analysis but they do not invalidate the simple qualitative picture presented here.

One difference between the exchange of the photon and the Z_0 is the couplings to both the electron and the nucleons. The photon has purely vector couplings, and couples only to protons at $Q^2 = 0$. We note that for the spinless nuclei considered here, the magnetic moments cannot contribute. Even though the Z_0 has both vector and axial vector couplings, the nuclei being considered are spinless, the net axial coupling to the nucleus is absent. In contrast to the case for photons, the Z_0 has a much larger coupling to the neutron than the proton. In addition, the Z_0 has a large axial coupling to the electron that results in a parity-violating amplitude.

The implication of the above is that the potential between an electron and a nucleus to a good approximation may be written

$$\hat{V}(r) = V(r) + \gamma_5 A(r) \tag{32}$$

where the usual electromagnetic vector potential is

$$V(r) = \int d^3r\prime Z\rho(r\prime)/|\vec{r} - \vec{r}\prime| \tag{33}$$

and where the charge density $\rho(r)$ is closely related to the point proton density $\rho_p(r)$ given by

$$Z\rho_p(r) = \sum_p \langle \psi_p^\dagger(r)\psi_p(r) \rangle. \tag{34}$$

The axial potential $A(r)$ depends also on the neutron density:

$$N\rho_n(r) = \sum_p \langle \psi_n^\dagger(r)\psi_n(r) \rangle. \tag{35}$$

It is given by

$$A(r) = \frac{G_F}{2^{3/2}}[(1 - 4\sin^2\theta_W)Z\rho_p(r) - N\rho_n(r)] \tag{36}$$

The axial potential has two important features:

1. It is much smaller than the vector potential, so it is best observed by measuring parity violation. It is of order one eV while $V(r)$ is of order MeV.

2. Since $\sin^2\theta_W \sim 0.23$, $(1 - 4\sin^2\theta_W)$ is small and $A(r)$ depends mainly on the neutron distribution $\rho_n(r)$.

As before, the electromagnetic cross section for scattering electrons with momentum transfer $q = (Q^2)^{1/2}$ is given by

$$\frac{d\sigma}{d\Omega} = \frac{d\sigma}{d\Omega}\bigg|_{\text{Mott}} |F_p(Q^2)|^2 \tag{37}$$

where

$$F_p(Q^2) = \frac{1}{4\pi}\int d^3r\, j_0(qr)\rho_p(r) \tag{38}$$

is the form factor for protons, where j_0 is the zero'th spherical Bessel function. From $F_p(Q^2)$, one may determine R_p. Note, we use the convention $Q^2 = -q_\mu^2 > 0$. One can also define a form factor for neutrons

$$F_n(Q^2) = \frac{1}{4\pi}\int d^3r\, j_0(qr)\rho_n(r) \tag{39}$$

Thus R_n may be determined if $F_n(Q^2)$ is known.

In Born approximation the parity-violating asymmetry involves the interference between $V(r)$ and $A(r)$. It is,

$$A_{LR} = \frac{G_F Q^2}{4\pi\alpha\sqrt{2}}\left[4\sin^2\theta_W - 1 + \frac{F_n(Q^2)}{F_p(Q^2)}\right] \tag{40}$$

The asymmetry is proportional to Q^2/M_Z^2 (since $G_F \propto M_Z^{-2}$) which is just the ratio of the propagators. Since 1-4sin$^2\theta_W$ is small and $F_p(Q^2)$ is known we see that A_{LR} directly measures $F_n(Q^2)$. Therefore, A_{LR} provides a practical method to cleanly measure the neutron form factor and hence R_n.

4   The Experimental Technique

In parity violating electron scattering experiments, one measures the helicity dependent left-right asymmetry in the scattering of longitudinally polarized relativistic electrons from unpolarized nuclear targets. The resulting asymmetries are small, requiring measurements with statistical and
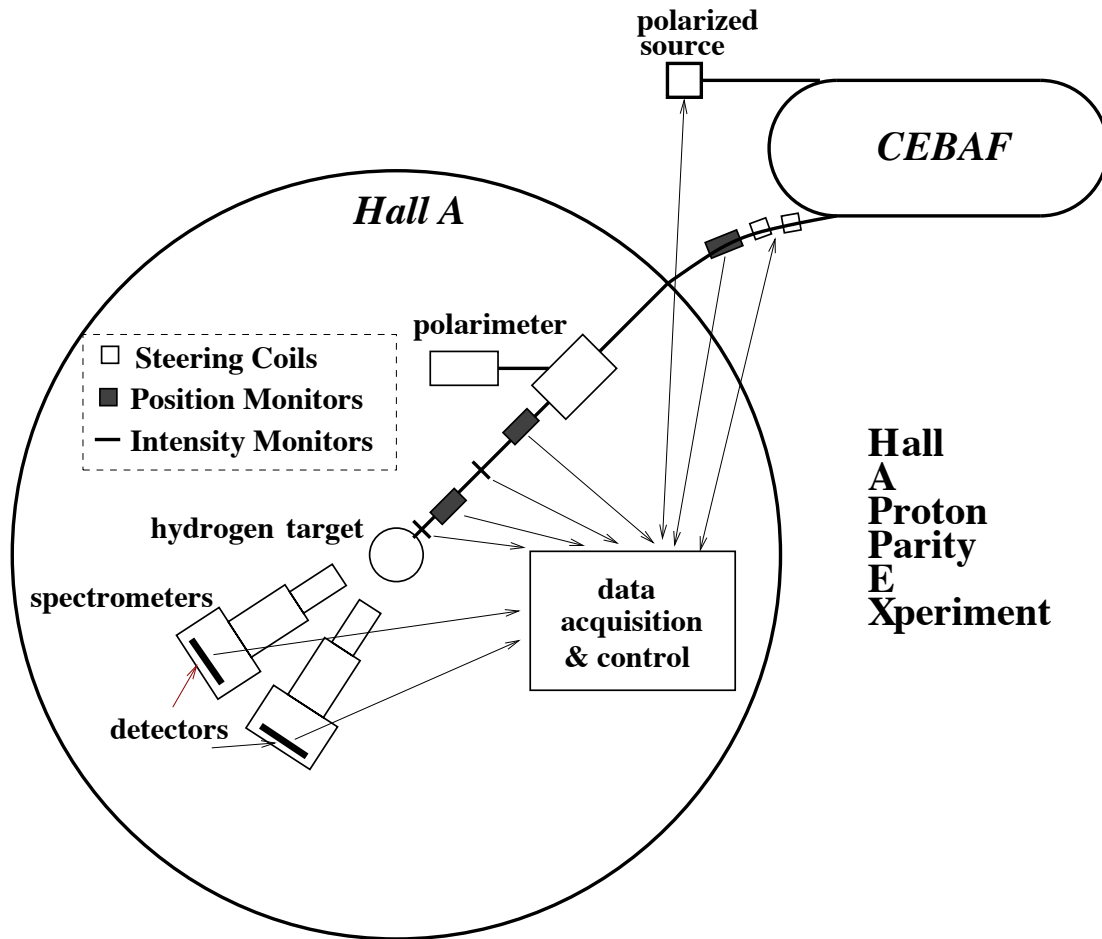
Figure 1: Schematic overview of the HAPPEX experiment at Jefferson Laboratory.

systematic errors substantially less than 1 part per million (ppm). This requirement leads to two overriding themes in the experimental technique; see Ref. [3] for a comprehensive discussion.

In the following, we briefly review salient features. First, the physical properties of the incident beam on target and the experimental environment as a whole must be identical for the left- and right-handed beams to a very high degree so as to minimize spurious asymmetries. Second, innovative flux counting techniques must be used in order to accumulate sufficient statistics.

Indeed, all successful experiments to date have used a GaAs photocathode to produce polarized electrons, with the ability to rapidly and randomly flip the sign of the electron beam polarization. The asymmetry is extracted by generating the incident electron beam as a pseudorandom time sequence of helicity "windows" and then measuring the fractional difference in the integrated scattered flux over window pairs of opposite helicity. Due to the high rates, the integrated scattered flux is typically obtained by flux counting, where the response of a charged particle detector that intercepts the scattered electrons is integrated over the duration of each helicity window.

The flux counting technique implies that spectrometers must be chosen that guide the scattered electrons of interest into a region that is otherwise free of background and detectors must be chosen whose response is dominated by the scattered electrons. Further, the electronics that record the detector signals must have sufficient resolution and be insensitive to electronic pickup.

Finally, it is important that random fluctuations from sources such as beam jitter, target density fluctuations and electronics noise are minimized.

Apart from random jitter, an important class of potential false asymmetries arise from helicity-correlated fluctuations in the physical properties of the beam, such as intensity, energy and trajectory. These properties are therefore monitored with high precision. The sensitivity of the scattered flux to fluctuations in the beam parameters are evaluated continuously and accurately.

To extract the physics asymmetry from the measured experimental raw asymmetry, one needs to measure the longitudinal polarization of the incident electron beam accurately. Electron beam polarimetry has matured over the past two decades. There are two main techniques: Compton polarimetry and Møller polarimetry each of which have advantages and disadvantages.

Figure 1 shows a schematic diagram of the important components of the HAPPEX experiment, as a specific example of the all the important components of a parity violation experiment, a detailed description of which can be found in Ref. [4]. Over the past 20 years, the experimental techniques employed to measure these tiny left-right asymmetries have been steadily refined such that statistical and systematic errors better than 1 part per billion (ppb) are possible [3]. Depending on the choice of target and kinematic variables, this has facilitated measurements in several important physics topics, such as many-body nuclear physics, nucleon structure and searches for physics beyond the standard model at the TeV scale.

5 Strangeness in Nucleons

5.1 Physics Motivation

One of the goals of modern nuclear physics is to incorporate sea quarks and gluons in a comprehensive description of nucleon substructure and to explore the connections of such a description with QCD. It has been known now for more than two decades with increasing precision that the quark spins are not the dominant contribution to the spin of the nucleon [5]. This prompted experimental and theoretical scrutiny of the role of sea quarks, especially strange quarks in describing the observables that characterize the bulk properties of the nucleon. One important way to cleanly isolate the effects of strange quarks is in the extraction of the vector strange matrix elements $\langle \overline{s} \gamma_\mu s \rangle$ in semi-leptonic neutral weak scattering [6].

An understanding of the role of strange quarks in the nucleon continues to have broad implications. The range of uncertainty in the strange-quark condensate $\langle \overline{s}s \rangle$ leads to an order of magnitude uncertainty in spin-independent scattering rates of dark matter candidates, while spin-dependent rates are uncertain to a factor of two given the range of uncertainty in the strange-quark contribution to nucleon spin, Δs [7]. The strange-sea asymmetry $s - \overline{s}$ is important for the interpretation of the NuTeV experiment [8, 9].

After it was realized that PVES can measure neutral weak form factors and extract $\langle \overline{s} \gamma_\mu s \rangle$ [10], several experiments were carried out, some of which presented evidence for non-zero strange form factors, albeit with marginal significance [11, 12, 13]. In contrast, the HAPPEX collaboration emphasized high statistical accuracy and small systematic uncertainties at a single value of Q^2 at a time, and has found results consistent with zero strangeness in each of several measurements at various values of Q^2 [4, 14].

The exact calculation of the strange form factors from QCD is challenging since it involves nonperturbative dynamics of sea quarks. Various model approaches have been used, such as chiral perturbation theory, quark models, lattice gauge theory, Skyrme models and dispersion relations [15, 16]. More recently, new predictions have become available from lattice calcula-

tions [17, 18]. It was determined that, in order to comprehensively probe for non-zero strange quark effects in the vector form factors, measurements over the range $0.1 < Q^2 < 1$ (GeV/c)^2, as well as forward and backward angle measurements off ^{1}H, ^{2}H and ^{4}He targets, are required.

The final measurement in the HAPPEX series known as HAPPEXIII was carried out in Fall 2009. The kinematics of HAPPEXIII were chosen to be particularly sensitive to the apparent effects reported in Ref. [11]. The experimental technique was similar to previous HAPPEX measurements [4]. A 100 μA continuous electron beam of longitudinally polarized electrons at 3.481 GeV was incident on a 25 cm long liquid hydrogen target. The twin Hall A High Resolution Spectrometers (HRS) [19] each accepted scattered electrons over a solid angle of 5 msr with an averaged polar angle of $\langle \theta \rangle \sim 13.7°$. Elastically scattered electrons from target protons were focused onto a calorimeter in each spectrometer; electrons from inelastic processes were not transported to the focal plane. Each calorimeter was composed of alternating layers of lead and lucite, with Čerenkov light from the electromagnetic shower collected by a photomultiplier tube. The physics run lasted about two months in late 2009 and sufficient statistics were accumulated to measure the raw asymmetry to better than 3.5%.

5.2 Physics Result and Implications

The final results were reported in a seminar at Jefferson Laboratory in February 2011 and has recently been submitted for publication in Physical Review Letters [20]. After all corrections and normalizations, the result was $A_{PV} = -23.80 \pm 0.78$ (stat)± 0.36 (syst) ppm at $Q^2 = 0.624$ (GeV/c)^2. If strange quarks did not contribute to the vector form factors, the asymmetry at that Q^2 is estimated to be $A_{NS} = -24.062 \pm 0.734$ ppm. Comparing the latter with the former, the specific combination of strange-quark electric and magnetic form factors are determined to be $G_E^s + 0.517\,G_M^s = 0.003 \pm 0.010 \pm 0.004 \pm 0.009$, where the error bars correspond to statistical, systematic, and electromagnetic form factor uncertainties, respectively.
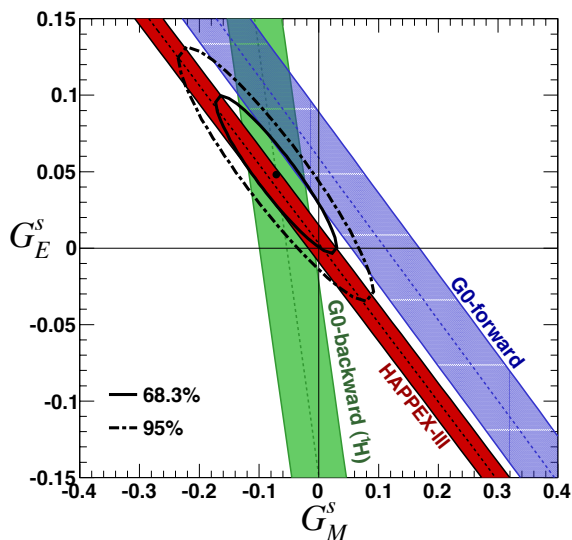

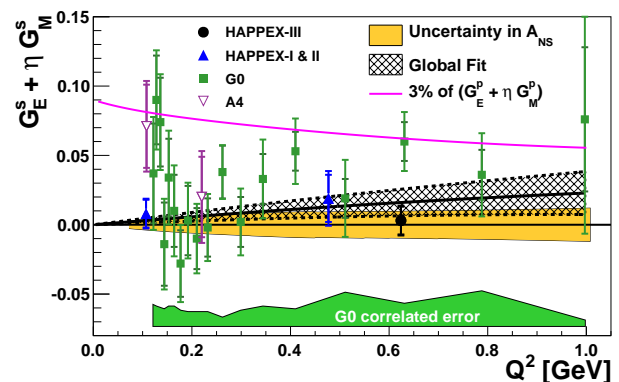Figure 2: Constraints on G_E^s and G_M^s at $Q^2 \sim 0.62$ (GeV/c)^2 from HAPPEXIII and G0 [11, 21].

Figure 3: Results of strange-quark vector form factors for all measurements of forward-angle scattering from the proton. The solid curve represents 3% of the corresponding nucleon electromagnetic form factor combination.

The constraints on the 2-D space spanned by G_E^s and G_M^s from all measurements near $Q^2 \sim 0.62$ (GeV/c)^2 are shown in Fig. 2. The experimental constraints at 1σ are represented by the

shaded bands indicating the combined statistical and experimental systematic error bars. The contours, representing the 68% and 95% uncertainty boundaries as indicated, combine all three measurements and also account for the uncertainties in A_{NS}. The independently separated values resulting from this fit are $G_E^s = 0.047 \pm 0.034$ and $G_M^s = -0.070 \pm 0.067$, with a correlation coefficient of -0.93. The combined constraint is consistent with $G_E^s = G_M^s = 0$.

Figure 3 shows all published data on the net strangeness contribution $G_E^s + \eta G_M^s$ in forward-angle scattering measurements from the proton versus Q^2. Here, $\eta = \tau G_M^p/(\epsilon G_E^p)$, and is approximately numerically equal to Q^2 over the range of the plot. Data from the HAPPEX [4, 14], G0 [11], and A4 [12, 13] collaborations are shown. On each data point, the error bars indicate both the statistical error and the quadrature sum of statistical and uncorrelated systematic error. For the G0 data, some systematic uncertainties are correlated between points with a magnitude indicated by the shaded region at the bottom of the plot. A shaded region around the zero-net-strangeness line represents the uncertainties in A_{NS} at 1σ; this uncertainty is not also included in the individual data points.

The cross-hatched region displays the 1σ region allowed by a leading-order fit in which G_M^s is taken to be constant and G_E^s is proportional to Q^2. The confidence level of the fit is 33%, demonstrating the reasonable self-consistency of the data. In contrast to the situation prior to this work, the HAPPEX-III point constrains the cross-hatched fit into significant overlap with the band corresponding to the uncertainty in A_{NS}, and just over 1σ from zero. Thus, the new result rules out large contributions from strange vector form factors with Q^2 behavior similar to that of the nucleon electromagnetic form factors.

6   The Neutron Skin of a Heavy Nucleus

While nuclear charge densities have been accurately measured with electron scattering, our knowledge of neutron densities comes primarily from hadron scattering experiments whose interpretations are model-dependent because of uncertainties in the strong interactions. PVES provides an independent probe of neutron densities that is free of most strong interaction uncertainties because the weak charge of the neutron is much larger than that of the proton [22]. The asymmetry A_{PV} in elastic electron scattering off a heavy spinless nucleus is proportional to the weak form factor, which in turn is very close to the Fourier transform of the neutron density. However, the Born approximation is not valid for a heavy nucleus and coulomb distortions must be accurately calculated to facilitate a robust extraction [23] .

A model-independent measurement of the radius of the neutron R_n to a fractional accuracy of 1% has important implications for many subfields. A number of models based on relativistic mean field theory have been developed to agree with the world data on nuclear charge distributions and other properties, but predict R_n values between 0.0 and 0.4 fm larger than R_p [24]. There is a strong correlation between R_n and the pressure of neutron matter at $\sim$2/3rd nuclear density, constraining the equation state EOS (pressure as a function of density) of neutron matter [25]. The correlation between R_n and the radius of a neutron star is also interesting [26]. The EOS of neutron matter is closely related to the symmetry energy S. There is a strong correlation between R_n and the density dependence of the symmetry energy $dS/d\rho$ (ρ is the baryon density). The symmetry energy S helps determine the composition of a neutron star; the transition density from solid crust to the liquid interior is strongly correlated to $R_n - R_p$ [27]. Finally, atomic parity violation (APV) measurements are sensitive to R_n [28, 29]. A future low energy test of the standard model may involve the combination of a precise APV measurement along with PVES to constrain

R_n. Alternatively, measuring APV over a range of isotopes can provide additional information on neutron densities [30].

Many details of a practical PVES experiment to measure neutron densities were spelled out [2], and formed the basis of the PREX proposal that took first data in Spring 2010. A 50 to 75 μA CW beam of longitudinally polarized 1 GeV electrons was incident on a 0.55 mm thick isotopically pure ^{208}Pb target. The optimum figure-of-merit requires that A_{PV} be measured with elastically scattered electrons in the range from 4 to 7 degrees, at a rate of more than 1 GHz, spatially separated from inelastic events from the first excited state at 2.5 MeV. The solution is to use a pair of septum magnets that bend the electrons into the acceptance of the high resolution spectrometers, whose minimum angle is 12.5° and whose hardware momentum resolution is 0.1%. The relative flux of the electrons over each 8.33 ms beam window of opposite longitudinal polarization was measured by directing the Cherenkov light from the quartz onto a photomultiplier tube and integrating the output using precision 18-bit ADCs. The magnitude of A_{PV} at the requisite low Q^2 of 0.01 (GeV/c)^2 is $\sim$ 700 ppb and a 3% measurement is required in order to determine R_n to 1%.

6.1   The PREXI Physics Run and Result

The first run of the PREX experiment took place between mid-March and late June 2010. The physics result was released in April 2011 and a publication is being prepared for submission to Physical Review Letters. The PREX design presented several technical challenges that needed to build on previous PVES experiments. The bulk of these issues were resolved during the run, and systematic control at the 10 ppb level and normalization control at the 1.5% level was demonstrated. The important technical achievements were:

- A new room temperature septum magnet was constructed and commissioned to bend scattered electrons in the range 4 to 7 degrees into the acceptance of the Hall A high resolution spectrometers.

- A new "double Wien filter" was installed, commissioned and tested during production running. This device provides a powerful new way to reverse the sign of the longitudinal polarization of the electron beam. All future parity experiments will make important use of this new innovation.

- The vector analyzing power for elastic scattering off ^{208}Pb was measured to be less than 0.5 ppm, which alleviates an important source of systematic error in the main A_{PV} measurement.

- A new "high-field" Møller polarimeter and a new green laser as the target for the Compton polarimeter were commissioned. The combined systematic error on the beam polarization was better than 1%, a record for a 1 GeV electron beam.

- A high power Pb target was commissioned and demonstrated to withstand a beam current of 70 μA for a period of a week. This is a major technical achievement, especially for carrying out a high flux parity-violation measurement given that the target becomes non-uniform and a subtle synchronization trick is needed to avoid increasing the statistical fluctuations.

- The detectors and electronics worked to the design specifications and achieved a noise floor that allowed the measurement of the 1 GHz flux to be "shot-noise limited".
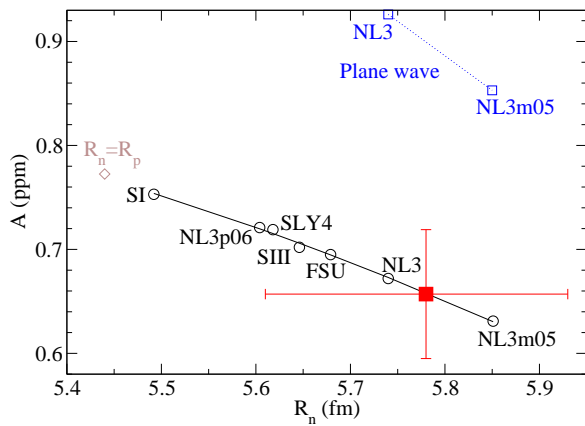
Figure 4: The PREX result (red square) vs R_n in ^{208}Pb. Distorted wave calculations for seven mean field neutron densities are circles [24], while the diamond shows the expectation SI neutron density rescaled so that $R_p = R_n$. The blue squares show the plane wave impulse approximation results.
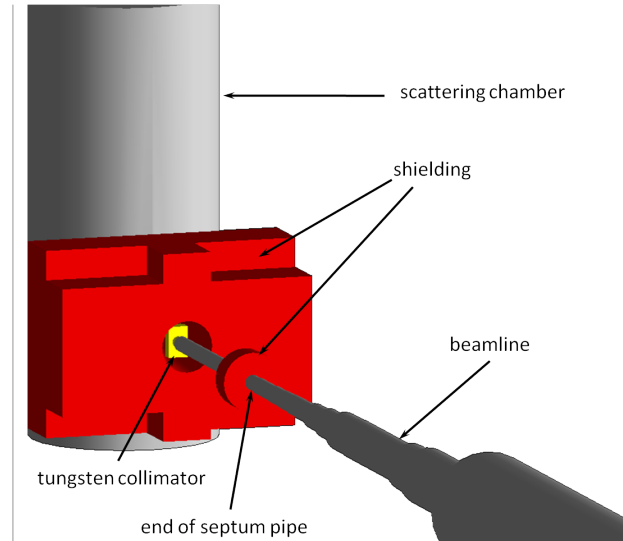

Figure 5: Toy geometry for the PREx II setup. Includes scattering chamber and stainless steel beampipe through the septum. The shielding fills the available space between the scattering chamber and the septum/attachments. The material is borated polyethylene. The detector is a large sphere which surrounds the entire geometry.

After corrections for beam fluctuations in the raw asymmetry analysis, the grand average was found to be 593 ± 50 parts per billion (ppb). After normalizing to the beam polarization and subtracting background, the PREX result is $A_{PV} = 657 \pm 60$ (stat) ± 13 (syst) ppb. The implications for R_n is demonstrated in Fig. 4. The measured result corresponds to a value for the neutron skin of $R_n - R_p = +0.34^{+0.15}_{-0.17}$ fm. The result demonstrates that the neutron RMS radius is 2σ larger than that of the protons. The result is consistent with all the models shown. In a future run, we plan to reduce the error bar by a factor of 3 to be able to discriminate between models and make predictions relevant to neutron stars. We discuss this followup proposal next.

6.2 The PREXII Proposal

While the PREX run was a technical success, only about 15% of the total statistics required for a 1% R_n determination was accumulated. In July 2012, the PREX collaboration submitted a new proposal to the Jefferson Laboratory Program Advisory Committee for an additional 25 days of beam time to complete the measurement to the desired level of precision. Several key improvements will be made to enhance the robustness of the apparatus and to achieve high data collection efficiency.

The proposal was approved with the highest rating. It is envisioned that the run would take place in calendar 2014. JLab is due to start commissioning the 12 GeV beams in 2013. In 2014, the nominal schedule calls for continued commissioning of the beams into Halls A and D. We propose to use the end of the commissioning period in Hall A in 2014 to complete the PREX data collection, which will require a period of two calendar months. It must be pointed out that this is

the only target of opportunity, since the beam energy cannot be lowered to 1 GeV once 12 GeV physics running begins in earnest in calendar 2015, when Halls B and C are scheduled to come on line.

7 Conclusions and Outlook

The twenty year search for strange quark vector form factors is coming to a close. While earlier measurements had suggested non-zero strange form factors, the new HAPPEX results leave little room for strangeness dynamics at low Q^2, a notion supported recent lattice gauge theory calculations [17, 18]. The A4 experiment plans to collect data at backward angles on both ^{1}H and ^{2}H targets at Q^2 of 0.1. They have already collected data at 0.6 GeV^2, and plan to release it soon. Both theoretically and experimentally, it has now become clear that strange form factors are no more than a few percent of the ordinary electromagnetic form factors.

For measurements of the neutron skin in heavy nuclei on the other hand, the future looks bright. The motivation to obtain a robust and model-independent determination of R_n over a range of nuclei will remain compelling for years to come. The PREX collaboration's followup proposal to obtain the remaining statistics required for a 1% R_n measurement at Jefferson Laboratory has been approved. Two other attractive nuclei to explore R_n measurements are ^{48}Ca and $^{120/124}$Sn. In general low Z nuclei tend to have a higher figure of merit due to the fact that the optimum Q^2 at which one must make the A_{PV} measurement tends to increase, and the figure of merit rises with the square of the asymmetry times the count rate [24].

^{48}Ca is particularly interesting because microscopic calculations may soon be feasible, which would allow R_n to be related to poorly studied 3-neutron forces. Sn isotopes are also interesting, since many of them have been used in heavy ion collisions to probe the density dependence of the symmetry energy, which has been shown to be related to R_n. It turns out that ^{48}Ca is an ideal measurement at Jefferson Laboratory with a similar configuration to that used for PREX, except that the beam energy would be raised to 2.2 GeV. This is one of the beam energies that would be possible to run simultaneously with a 11 GeV beam in another Hall.

It is interesting to consider measurements of Pb and Sn at Mainz in the future, adapting the apparatus that would be required for a high precision proton weak charge measurement. The loss in rate due to the lower beam energy is roughly compensated by the larger available solid angle. The momentum resolution that would be required is about 1%, and a system of baffles could be used to isolate elastic events while rejecting background from inelastics as well as from neutrals [31]. It will be very important to verify measurements of the same isotope in two different laboratories and also obtain consistent results on R_n from three different isotopes.

References

[1] K. Nakamura *et al.* (Particle Data Group), "Review of particle physics," J.Phys.G **G37**, p. 075021 (2010).

[2] C. Horowitz, S. Pollock, P. Souder, and R. Michaels, "Parity violating measurements of neutron densities," Phys.Rev. **C63**, p. 025501 (2001), `nucl-th/9912038`.

[3] K. S. Kumar and P. Souder, "Strange quarks and parity violation," Prog.Part.Nucl.Phys. **45**, pp. S333–S395 (2000).

[4] K. Aniol *et al.* (HAPPEX Collaboration), "Parity violating electroweak asymmetry in polarized-e p scattering," Phys.Rev. **C69**, p. 065501 (2004), `nucl-ex/0402004`.

[5] S. Bass, "The spin structure of the proton," Rev. Mod. Phys. **77**, p. 1257 (2005).

[6] D. B. Kaplan and A. Manohar, "Strange Matrix Elements in the Proton from Neutral Current Experiments," Nucl.Phys. **B310**, p. 527 (1988).

[7] J. R. Ellis, K. A. Olive, and C. Savage, "Hadronic Uncertainties in the Elastic Scattering of Supersymmetric Dark Matter," Phys.Rev. **D77**, p. 065026 (2008), `0801.3656`.

[8] H. Lai, P. M. Nadolsky, J. Pumplin, D. Stump, W. Tung, *et al.*, "The Strange parton distribution of the nucleon: Global analysis and applications," JHEP **0704**, p. 089 (2007), `hep-ph/0702268`.

[9] F. Olness, J. Pumplin, D. Stump, J. Huston, P. M. Nadolsky, *et al.*, "Neutrino dimuon production and the strangeness asymmetry of the nucleon," Eur.Phys.J. **C40**, pp. 145–156 (2005), `hep-ph/0312323`.

[10] R. McKeown, "Sensitivity of Polarized Elastic electron Proton Scattering to the Anomalous Baryon Number Magnetic Moment," Phys.Lett. **B219**, pp. 140–142 (1989).

[11] D. Armstrong *et al.* (G0 Collaboration), "Strange quark contributions to parity-violating asymmetries in the forward G0 electron-proton scattering experiment," Phys.Rev.Lett. **95**, p. 092001 (2005).

[12] F. Maas *et al.* (A4 Collaboration), "Measurement of strange quark contributions to the nucleon's form-factors at Q^2 = 0.230-(GeV/c)^2," Phys.Rev.Lett. **93**, p. 022002 (2004), `nucl-ex/0401019`.

[13] F. Maas, K. Aulenbacher, S. Baunack, L. Capozza, J. Diefenbach, *et al.*, "Evidence for strange quark contributions to the nucleon's form-factors at Q^2 = 0.108 (GeV/c)^2," Phys.Rev.Lett. **94**, p. 152001 (2005), `nucl-ex/0412030`.

[14] A. Acha *et al.* (HAPPEX collaboration), "Precision Measurements of the Nucleon Strange Form Factors at $Q^2 \sim 0.1$ GeV^2," Phys.Rev.Lett. **98**, p. 032301 (2007), `nucl-ex/0609002`.

[15] M. Musolf, T. Donnelly, J. Dubach, S. Pollock, S. Kowalski, *et al.*, "Intermediate-energy semileptonic probes of the hadronic neutral current," Phys.Rept. **239**, pp. 1–178 (1994).

[16] D. H. Beck and B. R. Holstein, "Nucleon structure and parity violating electron scattering," Int.J.Mod.Phys. **E10**, pp. 1–41 (2001), `hep-ph/0102053`.

[17] D. B. Leinweber, S. Boinepalli, A. W. Thomas, P. Wang, A. G. Williams, *et al.*, "Strange electric form-factor of the proton," Phys.Rev.Lett. **97**, p. 022001 (2006), ¡a href= http://www.abc.net.au/science/news/stories/2006/1734251.htm¿ ABC News Story¡/a¿, `hep-lat/0601025`.

[18] T. Doi, M. Deka, S.-J. Dong, T. Draper, K.-F. Liu, *et al.*, "Nucleon strangeness form factors from N(f) = 2+1 clover fermion lattice QCD," Phys.Rev. **D80**, p. 094503 (2009), `0903.3232`.

[19] J. Alcorn, B. Anderson, K. Aniol, J. Annand, L. Auerbach, *et al.*, "Basic Instrumentation for Hall A at Jefferson Lab," Nucl.Instrum.Meth. **A522**, pp. 294–346 (2004).

[20] Z. Ahmed *et al.* (HAPPEX collaboration), "New Precision Limit on the Strange Vector Form Factors of the Proton," (2011), * Temporary entry *, `1107.0913`.

[21] D. Androic *et al.* (G0 Collaboration), "Strange Quark Contributions to Parity-Violating Asymmetries in the Backward Angle G0 Electron Scattering Experiment," Phys.Rev.Lett. **104**, p. 012001 (2010), `0909.5107`.

[22] T. Donnelly, J. Dubach, and I. Sick, "Isospin Dependences in Parity Violating Electron Scattering," Nucl.Phys. **A503**, p. 589 (1989).

[23] C. Horowitz, "Parity violating elastic electron scattering and Coulomb distortions," Phys.Rev. **C57**, pp. 3430–3436 (1998), `nucl-th/9801011`.

[24] S. Ban, C. Horowitz, and R. Michaels, "Parity Violating Electron Scattering Measurements of Neutron Densities," (2010), `1010.3246`.

[25] B. Brown, "Neutron radii in nuclei and the neutron equation of state," Phys.Rev.Lett. **85**, pp. 5296–5299 (2000).

[26] C. J. Horowitz and J. Piekarewicz, "The Neutron radii of Pb-208 and neutron stars," Phys.Rev. **C64**, p. 062802 (2001), `nucl-th/0108036`.

[27] C. Horowitz and J. Piekarewicz, "Neutron star structure and the neutron radius of Pb-208," Phys.Rev.Lett. **86**, p. 5647 (2001), `astro-ph/0010227`.

[28] S. Pollock, E. Fortson, and L. Wilets, "Atomic parity nonconservation: Electroweak parameters and nuclear structure," Phys.Rev. **C46**, pp. 2587–2600 (1992), `nucl-th/9211004`.

[29] B. Brown, A. Derevianko, and V. Flambaum, "Calculations of the neutron skin and its effect in atomic parity violation," Phys.Rev. **C79**, p. 035501 (2009), `0804.4315`.

[30] K. Tsigutkin, D. Dounas-Frazer, A. Family, J. Stalnaker, V. Yashchuk, *et al.*, "Observation of a Large Atomic Parity Violation Effect in Ytterbium," Phys.Rev.Lett. **103**, p. 071601 (2009).

[31] P. Souder and R. Holmes, "New spectrometers for precision measurements of parity violation with polarized electrons," (1990).